International Journal of Environmental Sciences
ISSN: 2229-7359
Vol. 11 No. 7, 2025
https://www.theaspd.com/ijes.php

Green Synthesis of Gold Nanoparticles from Zingiber nigrum Leaves and their Efficacy in Photocatalytic Degradation of Toxic Dyes

Himanshu Singh[1], Raghvendra Singh Raghuvanshi[1], Abhishek Singh[1], Papu Kumar Naik[2], Ram Bilas Meena[3], Dhan Raj[3], Johny Lakra[4]
[1]Department of Chemistry, Udai Pratap Autonomous College, Varanasi, 221003 India
[2]Department of Earth and Environmental Science, Parul Institute of Applied Sciences, Parul University, Vadodara 391760, India
[3]Department of Chemistry, Government College Kota, Kota, 324001, India
[4]Department of Pharmacy, Maharishi Markandeshwar Deemed to be University, Mullana-Ambala, India
*Corresponding author: Email: rsraghuvanshiupc@hotmail.com

Abstract
The environmental friendliness of plants and their extracts makes them essential for the green manufacturing of nanoparticles. Plant extracts have been used to create a variety of metal nanoparticles. In this work, we report on an environmentally friendly approach of producing gold nanoparticles by utilizing aqueous extracts of Zingiber nigrum (ginger) leaves and assess their photocatalytic properties. The produced nanoparticles' capacity for photocatalysis and antioxidants was also evaluated. X-ray diffraction (XRD), Fourier transform infrared (FTIR) spectroscopy, and UV-Vis spectrophotometry were used to analyze the gold nanoparticles (Zn-AuNPs) that were synthesised by Zingiber nigrum. Powder XRD measurements verified the Zn-AuNPs' crystalline form. The Zn-AuNPs had an average particle size of 21.52 nm and were primarily spherical, according to micrographs obtained using high-resolution transmission electron microscopy (HRTEM). Polyphenolics and other functional groups that served as reducing and capping agents during the AuNP synthesis were discovered in the aqueous extract by FTIR spectral analysis. Significant antioxidant activity was demonstrated by these green-produced nanoparticles. The anthropogenic pollutant dyes methylene blue (MB) and rhodamine B (RhB) were catalyzed by Zn-AuNPs under UV radiation, with percent degradations of 93.25% and 97.64%, respectively. The photodegradation procedure adhered to a pseudo-first-order kinetic model. It has been suggested that the Zn on the Au nanoparticles effectively suppresses electron-hole recombination, which accounts for the observed photocatalytic activity of Zn-AuNPs. These findings support the notion that Zingiber nigrum is a viable bioresource for the production of gold nanoparticles with a wide range of environmental uses and is one of the novel features of this study.
Keywords: *Zingiber nigrum (ginger), Gold nanoparticles, Antioxidant, Photocatalysis.*

1. INTRODUCTION

Water is unquestionably a necessary resource for all facets of life, yet freshwater resources are currently scarce because of uneven distribution across nations and water contamination from industrial and agricultural processes [1]. The main contaminants that could be detected in the environment include inorganic pollutants including heavy metals, organic pollutants, and radioactive materials [2,3]. Toxic organic pollutants in particular are significant environmental contaminants that have posed a major risk to both human health and the ecosystem [4,5]. Combinations of several sources, including the widespread use of pesticides in agriculture, pharmaceuticals and the release of wastewater from industrial dye processes, lead to environmental organic pollution [6]. Methylene blue (MB), for example, is a recognised carcinogen with detrimental effects on both people and marine life [7]. Moreover, the extremely water-soluble organic cation dye rhodamine B dye (RhB) ($C_{28}H_{31}N_2O_3Cl$), a member of the xanthenes class, can cause irritation to the skin, eyes and lungs when in contact with humans [8]. In addition, it exhibits the chromophoric groups as well as a distinct carcinogenic and neurotoxic response. Since the textile dying is not a perfect process, at least 10% of the colour is lost to sewage washout. Thus, it is inevitable that these dyes will be removed or degraded quickly and effectively [9].

Unfortunately, organic debris, microbes, and hazardous compounds cannot be eliminated by the decades-old water treatment methods [10,11]. Because of nanomaterials' low cost, great efficacy in eliminating different types of contaminants, and reusability, researchers started looking for and relying on suitable alternatives in

wastewater treatment [12,13]. Numerous nanomaterials, including zeolites, dendrimers, metallic nanoparticles, carbon nanotubes (CNTs), and nanomembranes, are being widely exploited to improve wastewater treatment routes [14,15]. Several researchers have reported on the breakdown of MB using photocatalytic assemblies based on nanomaterials too [16-19].

The intriguing changes in the characteristics of the noble metals at the nanoscale are particularly intriguing [20,21]. Gold, among the noble metals, has garnered significant attention due to its fascinating optical, chemical, and electrical properties, along with its diverse applications in lubricants, cosmetics, pharmacology, drug delivery, and catalysis, among other fields [22,23]. Moreover, due to the very large surface area and diminutive particle size of AuNPs, they are commonly employed in photocatalytic and catalytic processes for the elimination of organic pollutants [24]. These characteristics, however, differ depending on the size and shape of the gold nanoparticles. Hexagonal and pentagonal gold nanoparticles are believed to possess higher catalytic activity compared to other geometries, due to their more reactive surfaces [25]. Biosynthesis of nanostructures by plants and microbes, on the other hand, has been aroused as a safer, less expensive, and more sustainable method [26,27]. However, using microorganisms necessitates careful handling and maintenance in the cultivation and growth of these organisms, which adds to the costs [28]. The plant extracts, which contain phytochemicals including phenols, flavonoids, and terpenoids, were more efficient, cost-effective, and simple for synthesizing metal and metal oxide nanoparticles in a single-step green synthesis process. The compounds including phenols, flavonoids, and terpenoids in plant extracts reduce and stabilize nanoparticle synthesis [29].

Gold nanoparticles have recently been synthesized using *Mussaenda glabrata* [30], *Galaxaura elongate* [31], *Plumeria alba* [32], *Alpinia nigra* [33], and *Tecoma capensis* [34]. The herbaceous perennial ginger (*Zingiber officinale*) has aerial shoots, fibrous roots, and a rhizome. *Zingiber officinale*, sometimes known as ginger, has been used for centuries in India and China as a spice and medicinal herb. Today, it is one of the most extensively used spices in the world and is used in a broad variety of foods, beverages, pharmaceuticals, and personal care products. Ginger has long been used as a traditional medicine in Southeast Asia to cure fevers, coughs, sore throats, and other ailments [35]. Numerous significant phytoconstituents, including phenols, glycosides, terpenoids, alkaloids and flavonoids, have been found in studies on leaves and seeds [36,37]. The chemical constituents of ginger are known to have positive health effects; these include their anti-inflammatory and antioxidant properties, as well as their potential to function as immunomodulators [38]. We have hypothesized that *Zingiber nigrum* leaves could function as a useful reducing and stabilizing agent during the manufacture of gold nanoparticles, based on these results. The manufacture of gold nanoparticles mediated by *Zingiber nigrum* leaves and their antioxidant and photocatalytic capabilities are reported in this paper, along with a simple green method for doing so.

2. MATERIALS AND METHOD

2.1 Chemicals and reagents: All reagents used in this study were of analytical grade including gold tetrachloroaurate solution ($HAuCl_4 \cdot 3H_2O$), 2,2-diphenyl-1-picrylhydrazyl (DPPH) (99%), ascorbic acid, and methylene blue (MB) and rhodamine B (RhB) purchased from Merck, USA. Dimethyl Sulphoxide (DMSO) was obtained from Hi Media (India). All the reagents were of analytical grade and used without any further purification.

2.2 **Characterization:** Using a Hitachi U3900 UV-Vis spectrophotometer, the formation of gold nanoparticles were observed at wavelengths ranging from 300 to 800 nm. The Zn-AuNPs' morphological shape and size were assessed using a JEM-2100 HRTEM, a high-resolution transmission electron microscope. After placing a drop of the colloidal solution at a potential of 20 kV, the copper grid was allowed to dry fully. To obtain the Zn-AuNPSs powder, the gold nanoparticles were centrifuged for 20 min at 10,000 rpm, collected and dried the pellets. Scanning Electron Microscopy (SEM) images were captured with the ZEISS SIGMA instrument and Energy Dispersive X-ray (EDX) images acquired with the OXFORD X MAXN instrument in order to examine the morphology of the Au nanoparticles. KBr pellets were used in an FTIR spectrophotometer of the Perkin-Elmer 2000 series to analyse the functional groups present within the region of 4000–600 cm_1. Zn-AuNPs' crystalline nature was examined using a Cu*K*α X-ray radiation (λ = 1.54056 Å) in a Rigaku X-ray diffractometer (model: ULTIMA IV, Rigaku, Japan) with a generator voltage of 40 kV and a generator current

of 40 mA. At a scanning rate of 2°/min, the scanning was carried out in the 20°–80° range. Using the JEOL model JSM-IT100 energy-dispersive X-ray spectroscopy (EDX), the elemental composition was analyzed.

2.3 Preparation of plant extract of *Zingiber nigrum*: *Zingiber nigrum* leaves were rinsed five or six times with double distilled water to get rid of any undesired elements and pollutants and then dried for 24 hours at room temperature (27 °C) before being baked for an entire night at 60 °C. A fine powder was obtained by grinding the dry leaves in a stainless-steel mixer. After dissolving 10 g of the resulting powder in 100 mL of distilled water, the mixture was agitated and heated for about 30 min until it boiled. After filtering the heated solution, the filtrate extract was kept for later use at 4.0 °C.

2.4 Biosynthesis of Zingiber nigrum-gold nanoparticles (Zn-AuNPs): $HAuCl_4 \cdot 3H_2O$ (1 mL, 0.011 M) was gradually mixed with 10mL of extracted Z. nigrum leaves after constant heating (to 95 °C) and stirred for 10 min. After 15 min, a colour shift from the original light yellow to a dark purple red tone was obtained, which confirmed the development of Au nanoparticles. Centrifuged the *Zingiber nigrum*-AuNPs colloidal solution, the precipitated pellets was collected and washed with double-distilled water completed the purification process. After AuNPs were synthesised, this process was carried out four times to purify them. The resulting colloidal solution was then kept for further use at 4 °C.

2.5. Antioxdant activity: The DPPH (2, 2-diphenyl-1-picrylhydrazyl) assay was used to assess the Zn-AuNPs' capacity to scavenge free radicals and ascertain the antioxidant efficacy of *Zingiber nigrum*-gold nanoparticles (Zn-AuNPs) and leaf extract, in accordance with the reported methodology [39]. In brief, a DPPH solution at 0.3 mM in methanol was prepared. The Zn-Au-NPs solution was prepared as a stock solution in methanol. The test samples were prepared from the stock solution, with concentrations ranging from 25 µg/ml to 400 µg/ml. Following the addition of 1 mL of the DPPH reagent and thorough agitation of the mixture, it was allowed to incubate for 50 min in dark. Methanol was used as the blank and ascorbic acid as the positive standard. Using a Hitachi U3900 UV-Vis Spectrophotometer, the absorbance was measured at 517 nm. The following formula was used to get the DPPH radical's percent inhibition:

$$\text{Inhibition (\%)} = \frac{\text{Absorbance of control} - \text{Absorbance of sample}}{\text{Absorbance of control}} \times 100$$

Zingiber nigrum leaves extract and *Zingiber nigrum*-gold nanoparticles (Zn-AuNPs) at 517 nm are examples of the test solution's absorbance in the presence of antioxidants, whereas the control solution's absorbance is the absorbance in the absence of antioxidants.

2.6. Photocatalytic activity: To analyze the photocatalytic activity of Zn-AuNP nanoparticles, the rhodamine B (RhB) and methylene blue (MB) dyes were decolorized in the presence of UV light. An immersion well pyrex glass photoreactor (inner and outer jacket) with a magnetic bar, a water-circulating jacket, and a molecular oxygen opening was used for the photocatalytic investigations. The region was illuminated with a 125 W medium-pressure mercury lamp (Philips). By exposing the RhB and MB aqueous solutions to varying concentration of Zn-AuNPs nanoparticles, the optimum catalyst dosage was determined. To achieve the RhB and MB dyes and nano-catalyst surface adsorption-desorption equilibrium, 180 mL of a separate (0.06 mM) solution containing produced nanocatalysts (1 g L^{-1}) were magnetically whirled in dark for atleast 30 min in the presence of ambient oxygen. The irradiation procedure started once the first aliquot (5 mL, 0 min) had reached equilibrium. The 5 mL aliquots were obtained during the irradiation at regular intervals of 15, 45, 60, 90 and 120 min, were centrifuged and then analyzed. Using a standard calibration curve based on the dye's absorbance at several known values, the concentration of the dye was ascertained. Blank controls for the experiment were dye solutions devoid of the catalyst. During the experiment, another control set used dyes containing Zn-AuNPs without the use of a catalyst. Using a halogen linear lamp (500 W, 9500 Lumens) as a light source and similar experimental settings as previously mentioned, the decolorization of RhB and MB dye in the presence of visible light was used to investigate the photocatalytic activity of the Zn-AuNPs nanoparticles. The percent degradation of each dye was calculated using the formula:

$$\text{Degradation (\%)} = \frac{(A_o - A)}{A_o} \times 100$$

where A_0 denotes the absorbance of the blank dye solution (exposed to sunlight without the addition of the nanoparticles) and A denotes the absorbance of the test solutions (containing the Zn-AuNPs and exposed to sunlight) recorded at different time intervals [40,41].

3 RESULT AND DISCUSSION

3.1 UV–Vis spectroscopy: UV-VIS absorption spectroscopy was used to track the development of gold nanoparticles. The absorption spectra show that the surface plasmon resonance (SPR) band corresponding to AuNPs is located between 530 and 570 nm. The aqueous extract of *Zingiber nigrum* in the current investigation underwent a colour change from light brown to dark brown after gold ions (Au^{2+}) solution was added, and a surface plasmon resonance peak at 515 nm indicated the phyto-fabrication of Zn-AuNPs [Fig. 1a]. The obtained results were consistent with those reported in other investigations that looked into the green synthesis of AuNPs using different plant extracts [42,43]. The dimensions, morphology and interaction of the particles with the medium determine the displacement of the SPR bands [44].

3.2 XRD analysis: Powder XRD measurements verified the crystallinity of green synthesized AuNPs. The Bragg's reflection with 2θ values of 38.40°, 44.38 °, 64.89°, 78.86° and 82.81° is indexed to the (111), (200), (220), (311), and (222) planes of the face-centered cubic (fcc) crystal structure, as demonstrated by the XRD diffractogram in [Fig.1b], which validates the crystalline nature of the Au-NPs with JCPDS No. 001-1172 [45]. The most intense peak corresponds to the (111) plane, indicating that this is the direction in which the nanoparticles are growing most frequently [42]. Additionally, following the photocatalytic degradation of both dyes, the recovered catalyst (Zn-AuNPs MB and Zn-AuNPs RhB) exhibits peaks comparable to the fresh catalyst, indicating that it does not experience any structural changes during the reaction process which is reusable also [43].

3.3 **FTIR analysis:** Functional groups that are probably assisting in the reduction and stabilization of photosynthesized nanomaterials are typically identified using FT-IR. FTIR spectroscopy was used to identify the potential biomolecules in Zn-AuNPs that served as stabilizing and reducing agents during the nanoparticle's formation [46]. The Zingiber nigrum extract's infrared spectrum [Fig. 1c] showed several peaks that correspond to the different functional groups. The amide N-H stretch and OH stretching of the alcohol/phenol group, which are present in the Zn aqueous extract and Zn-AuNPs, respectively, are responsible for the peak at 3434.2 cm^{-1}. In the Zn-AuNPs spectra, the functional group also observed an H-bonded O-H peak at 3201 cm^{-1} that shifted to 3287 cm^{-1} with significantly lesser intensity as shown in Fig. 1d. The Zn-AuNPs spectra showed a doublet C-H stretch at 2930 and 2850 cm^{-1}, which was absent from the *Zingiber nigrum* extract. The C=C band and C–H bending were found in the *Zingiber nigrum* extract spectra at 1602 and 1400 cm^{-1}, respectively. After that, they were moved to the Zn-AuNP spectra at lesser intensities to 1629 and 1428 cm^{-1}. The amine group's C-N stretching is shown by the band that appears at 1384.6 cm^{-1}. In Zn-AuNPs, C-O stretching first emerged at 1095 cm^{-1}, which it moved to a lower wavenumber of 1075 cm^{-1}. Thus, it was determined that a variety of phytoconstituents, particularly those with O-H functional groups

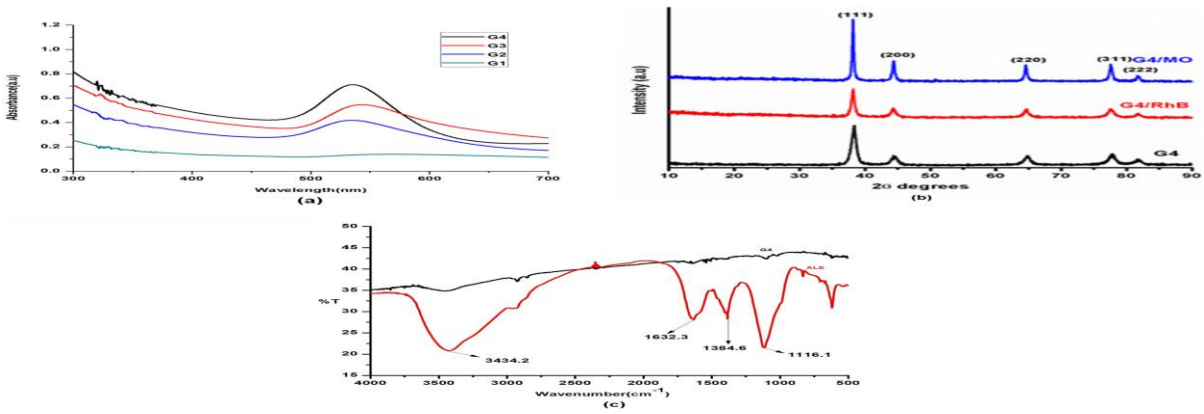

Fig. 1

including terpenoids, alkaloids, flavonoids, glycosides and tannins, were in charge of the stabilization and reduction of Zn-AuNPs. The FTIR spectrum exhibited a prominent band at 1116.1 cm^{-1}, which is attributed to the C=O stretching vibrations characteristic of polyphenols, alcohols and ethers. This suggests that proteins and polyphenolic compounds played an essential role in both stabilizing the synthesized gold nanoparticles and facilitating the reduction of Au^{3+} ions to metallic Au^{0}. These findings are consistent with the work of Tausif *et al.* [47,48], who demonstrated that phenolic compounds are responsible for the effective conversion of gold ions into gold nanoparticles (AuNPs), confirming the role of these biomolecules in nanoparticle synthesis. The position and intensity of peaks change when the spectra of Zn and Zn-AuNPs (Figs. 1c-d) are compared, suggesting that these biomolecules were involved in the reduction of $HAuCl_4$ and stabilisation of the Au-NPs [47]. The observed key FT-IR peaks are summarised in Table-1.

3.4 SEM analysis: The shape and structure of the nanoparticles were analyzed using a field emission scanning electron microscope (FE-SEM). The majority of the nanoparticles in Fig. 2a are spherical, according to the SEM image. The presence of elemental gold is demonstrated by the elemental technique of the energy-dispersive X-ray (EDX) spectrum (Fig. 2b). Furthermore, the presence of C, O and Al in the spectrum indicates the existence of phytochemicals. According to Fig. 2b, the EDX analysis demonstrated the photoreduction of gold chloroaurate ($HAuCl_4$) into Zn-AuNPs using strong signals of elemental gold atoms found at many energy levels, mostly at 2.4 KeV but also at 2.9, 8.6, 9.9, 11.7 and 13.7 KeV. In addition, signs for other elements that are thought to have a plant origin, such carbon and oxygen, were observed. The copper signals that might have come from the carbon-coated copper grid employed in this investigation were found. These results were consistent with earlier investigations [49,50].

Table 1. Summarizing the key peaks, their range, intensity changes, and significance in Zn and Zn-AuNPs based on the provided FT-IR analysis:

Peak (cm^{-1})	Zn Extract	Zn-AuNPs	Functional Group	Intensity Change	Significance
3434.2	Present	Present	Amide N-H stretch or O-H stretch	Similar	Indicates involvement of amide or hydroxyl groups in reduction and stabilization.
3201	Present	Shifted to 3287	H-bonded O-H	Lower in Zn-AuNPs	Change in the hydrogen bonding environment is important for stabilization.
2930, 2850	Absent	Present	C-H stretch	Present in Zn-AuNPs only	New C-H interactions indicate successful synthesis and stabilization.
1602	Present	Shifted to 1629	C=C stretch	Lower in Zn-AuNPs	Interaction and stabilization by polyphenolic compounds.
1400	Present	Shifted to 1428	C-H bending	Lower in Zn-AuNPs	Involvement of phenolic compounds in stabilization.
1384.6	Present	Present	C-N stretching (amine groups)	Similar	Indicates the presence of amine groups contributing to nanoparticle synthesis.
1095	Present	Shifted to 1075	C-O stretching	Lower in Zn-AuNPs	Changes in the bonding environment, contribute to the stabilization of nanoparticles.
1116.1	Present	Present	C=O stretching (ethers, alcohols, polyphenols)	Same intensity	Involvement of polyphenolic compounds and proteins in reduction and stabilization.

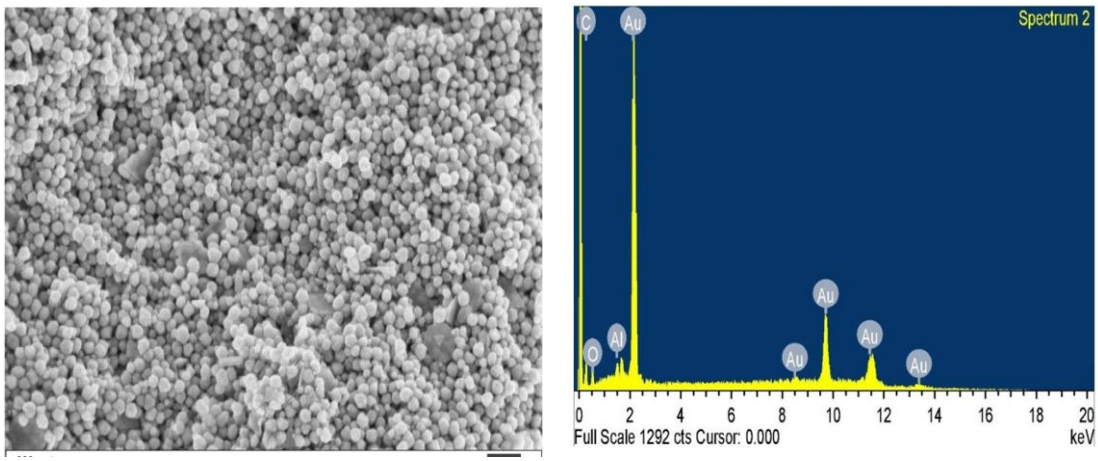

Fig. 2. (a) FE-SEM image of G4 showing uniform distribution of nanoparticles, (b) EDX spectrum of G4 showing the presence of elemental Au along with C, O and Al.

3.5 HRTEM analysis: To ascertain the size, shape, and other morphological properties of nanoparticles, the technique of microscopy was employed. Zn-AuNPs were found to range in size from 8 nm to over 40 nm, with a spherical form being the most common, according to HRTEM examination (Fig. 3a–c). A histogram showing the various Zn-AuNP particle sizes based on the HRTEM images is shown in Fig. 3.d, and it shows that the average particle size is between 25 and 30 nm with about 29.9%. Other shapes were also found, including hexagonal, rhombohedral, triangular and other irregular shapes. It has been previously demonstrated that the varied phytoconstituents found in plant extracts are primarily responsible for the distinct shapes of phytofabricated AuNPs [51]. Since the various phytoconstituents found in the extract of zinc leaves, including terpenoids, alkaloids, flavonoids, glycosides, and tannins, may have varying potentials for reduction, this could affect the reduction process and lead to the development of distinct forms of AuNPs [51,52].

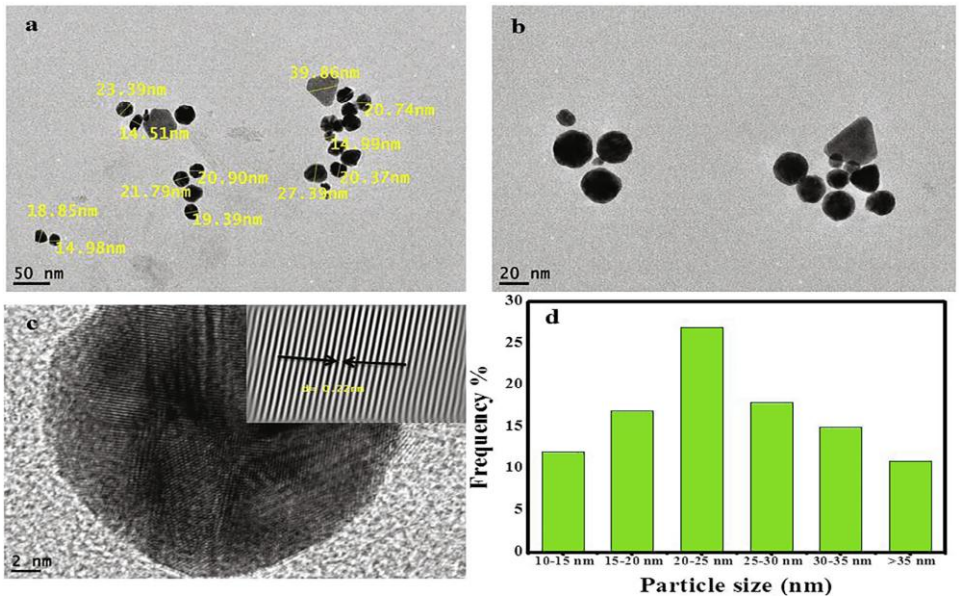

Fig. 3 (a-c) HRTEM images of *Zingiber nigrum*-AuNPs (d) Particle size distribution histogram of *Z. nigrum*-AuNPs

3.6. Antioxidant potential of Zn-AuNPs: It has been established that metallic nanoparticles are vital in the fight against harmful free radicals like DPPH [53,54]. As a result, it was determined that the OH-DPPH solution was converted to the non-radical form of DPPH-H, which allowed for the elimination of DPPH by the use of antioxidants such as Zn-AuNPs and Zn leaf extract, which served as donors of electrons or hydrogen. Using a spectrophotometer, the assay was designed to quantify the change in DPPH concentration brought about by DPPH's reaction with Zn-AuNPs and Zn leaf extract. Measured by changes in optical absorbance at 517 nm, the DPPH was decoloured as a result of getting an electron from Zn-AuNPs or Zn leaf extract. When antioxidants are utilized to stop the oxidative chain reaction from starting, non-reactive radicals are produced. This is known as the antioxidant activity notion. Additionally, it has been discovered that AuNPs, particularly when synthesised using a green process, have strong antioxidant capacity to prevent oxidative damage [55]. As was shown in earlier research [56], the antioxidant activity of Zn-AuNPs is dependent on the Zn phytoconstituents, such as alkaloids, which are encasing the nanoparticles. This is because the current study's zinc aqueous extract was shown to be an extremely effective antioxidant. Fig. 4 in this investigation demonstrated that, in a concentration-dependent manner, all of the antioxidant samples exhibited inhibitory action against the DPPH free radical. At a concentration of 100 μg/mL, Zn-AuNPs and Zn aqueous extract both demonstrated strong DPPH scavenging efficacies of approximately 86.62 and 70.83%, respectively. Since vitamin C could only remove 55.04% of DPPH at the same concentration when employed as a reference (positive control), its scavenging activity was shown to be less powerful. The fast reduction of gold ions into Zn-AuNPs following the addition of the extract suggested that the Zn aqueous extract was a superior antioxidant than Zn-AuNPs [57]. Zn-AuNPs have a strong antioxidant efficacy, as shown in Table2.

Table 2. Comparison between the antioxidant efficiency of *Zn*-AuNPs synthesized in the current study and other metal nanoparticles prepared in other studies.

Nanoparticle Type	Plant extract	Scavenging Activity (%)	Reference
AuNPs	*Moringa oleifera*	82 ± 0.5	[58]
ZnONPs	*Eucalyptus globulus*	70.0	[59]
CuNPs	*Ceropegia debilis*	51	[60]
AuNPs	*Crassocephalum rubens*	45	[61]
AuNPs	endophytic Cladosporium species	10	[62]
AuNPs	mannosylerythritol lipid	50	[63]
AuNPs	*Tecoma capensis*	85	[64]
AuNPs	*Zingiber nigrum*	86.62	Current study

3.9. Photocatalytic Degradation of methylene blue (MB) and rhodamine B (RhB) dyes: Popular water-soluble dyes methylene blue and rhodamine B are widely used in a variety of industries, including the textile, printing, paper, pharmaceutical, painting, leather, and food industries [65,66]. The absorption maxima of methylene blue and rhodamine B were centred at around 465 and 558 nm, respectively. As can be seen in Figs. 5a and 5c, the primary absorption peak in both cases steadily dropped until it neared the baseline. Furthermore, Figs. 5b and 5d, respectively depict the curve of $\ln(A/A_0)$ vs. time for the catalytic degradation of the dye solutions employing Zn-AuNPs. The rate constant determined by utilising Fig. 5b is found to be 1.463×10^{-2} min^{-1}. The experimental data fits the pseudo first-order kinetic model well, as indicated by the regression coefficient value of 0.975 for the same. In a similar manner, 1.495×10^{-2} min^{-1} is the rate constant for the breakdown of rhodamine B. In this instance, the regression coefficient value of 0.995 indicates unequivocally that the kinetics follow the pseudo-first order.

Through reductive breakdown, gold nanoparticles help in the bioremediation of wastewater containing dangerous dyes such as rhodamine B and methylene blue. There are three steps in the overall process. When gold atoms are exposed to UV radiation, their electrons are excited from the low-energy valence band to the high-energy conduction band, starting the deterioration process. The electrons in gold atoms receive just the proper amount of energy from UV light to overcome the nucleus's pull and enter the conduction band. The organic dye molecule absorbs electrons from the gold surface's valence band, which causes the dye to break down and eventually turn into a mineral. The % degradation for each dye solution was computed and displayed against time to examine the relative reactivity of Zn-AuNPs against the two dye solutions (Fig. 6). The graph clearly show that the gold nanoparticles were more effective against rhodamine B and the maximum % degradation was achieved at 97.64% after 120 min. On the other hand, the % degradation of methylene blue orange was 93.25% after 120 min.

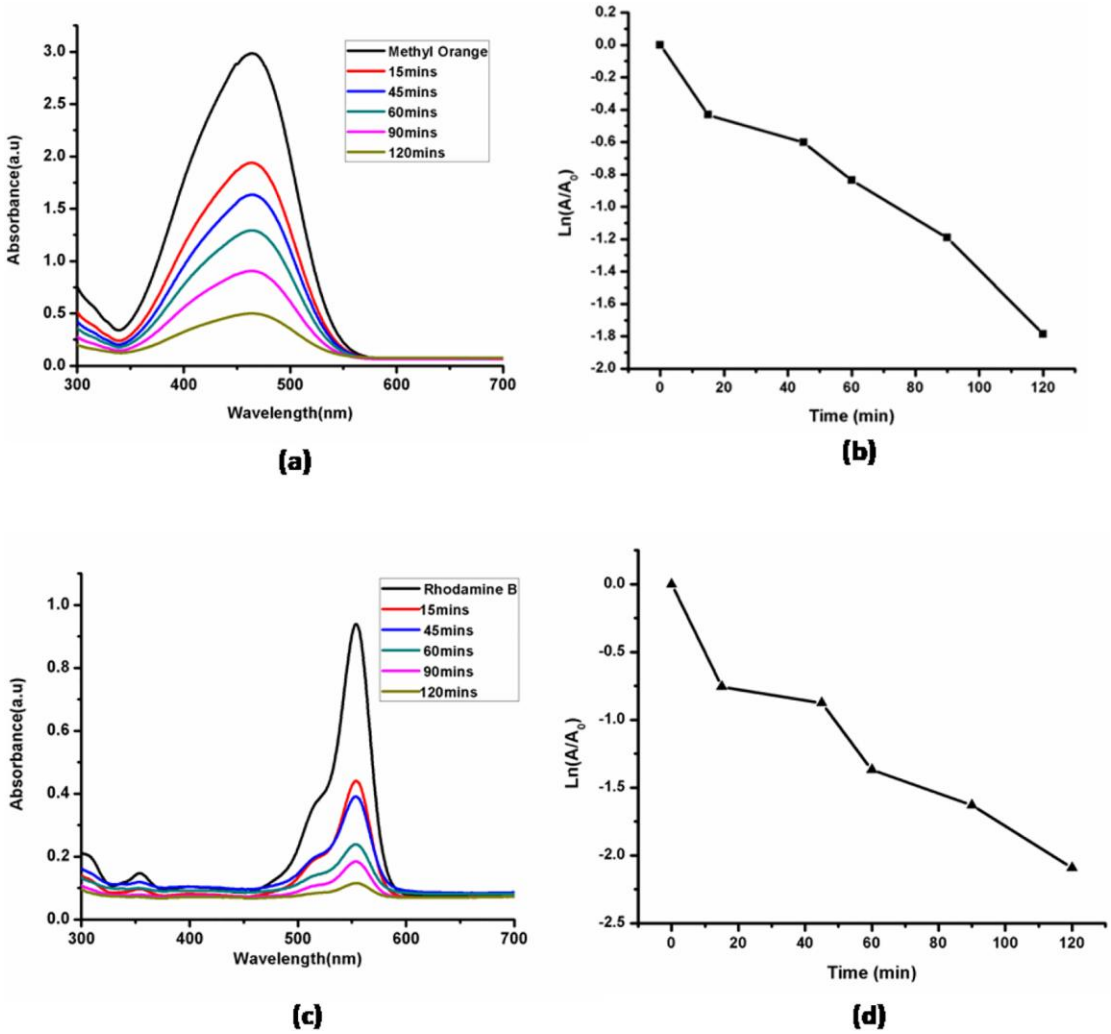

Fig. 5. (a) UV–visible spectra of Methylene blue degradation in the presence of ZN-AuNPs, (b) Ln (A/A0) *vs* Time for catalytic degradation of Methylene blue, (c) UV–visible spectra of rhodamine B degradation in the presence of Zn-AuNPs, (d) $\ln(A/A_0)$ *versus* time for catalytic degradation of rhodamine B. The regression coefficient for methylene blue is 0.965 while that for rhodamine B is 0.985.

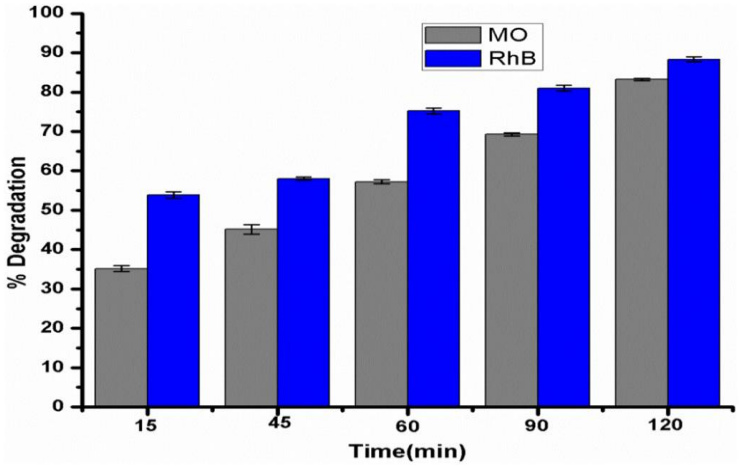

Fig. 6. Plot of % Degradation of methylene blue and rhodamine B dyes against time

Mechanism: A mechanism for the photodegradation of MB and RhB dyes as follows in which the utilization of *Zn*-AuNPs as a photocatalyst has resulted in the degradation of both dyes (MB and RhB) into simple, non-toxic, and inorganic products such as CO_2 and H_2O. The photodegradation process of dyes is simply clarified by the following equations [72]:

$$(MB\ or\ RhB)\ Dye + h\nu \rightarrow Dye^* \quad (1)$$

$$Dye^* + [Zn\text{-}AuNPs] \rightarrow e^-_{cb}[Zn\text{-}AuNPs] + h^+_{vb}[Zn\text{-}AuNPs] \quad (2)$$

$$(H_2O \rightarrow H^+ + OH^-) + h^+_{vb}[Zn\text{-}AuNPs] \rightarrow H^+ + HO\bullet \quad (3)$$

$$(O_2 + e^-_{cb}[\ Zn\text{-}AuNPs]) \rightarrow O^-_2 + (H^+ + OH^-) \rightarrow HOO\bullet + OH^- \quad (4)$$

$$HOO\bullet + OH^- + h^+_{vb}[Zn\text{-}AuNPs] \rightarrow HO\bullet \quad (5)$$

$$Dye + (HO\bullet O^{\bullet -}_2\ and/O_2 \rightarrow degraded\ products \quad (6)$$

$$Dye + h^+ \rightarrow Oxidation\ products \quad (7)$$

$$Dye + e^- \rightarrow Reduction\ products \quad (8)$$

By absorbing UV light, MG adsorbed on the surface of *Zn*-AuNPs became excited and commenced to donate its electrons to the conduction band of Zn-AuNPs. Afterward, these electrons were scavenged by dissolved oxygen and resulted in the formation of highly reactive superoxide oxygen radical (O_2*). Moreover, the O_2* can react with H_2O adsorbed on the MG surface to form H_2O_2, which is promptly transformed into OH*. Eventually, both O_2* and OH* led to the degradation of MG into CO_2, H_2O and byproducts.

4. CONCLUSION

According to present research, *Zingiber nigrum* leaf extract was used to synthesize gold nanoparticles by acting as both a stabilising and reducing agent. The pristine crystalline nature of the gold nanoparticles is shown by their characterisation. The AuNPs indicated the phyto-fabrication of Zn-AuNPs; they were primarily spherical and had a surface plasmon peak at 515 nm. The crystalline nature of Zn-AuNPs with an FCC structure is confirmed by PXRD. While changes in the position and intensity of peaks suggest that these Zn biomolecules were engaged in the reduction of $HAuCl_4$ and stabilisation of the Au-NPs, observed peaks in FT-IR spectra validate the production of Zn-AuNPs. Synthesised nanoparticles are shaped like triangles, rhomboids, hexagons, and irregular shapes, according to SEM, EDX, and HRTEM. Zn-AuNPs and Zn aqueous extract both demonstrated strong DPPH scavenging efficacies of approximately 70.83% and 86.62%, respectively, in comparison to vitamin C, which eliminated just 55.04% of DPPH. Under the presence of a UV lamp, Zn-AuNPs effectively catalyzed the degradation of the dyes rhodamine B and methylene blue. Rhodamine B and Methylene blue had the highest percentage of degradation, 93.25% and 97.64%, respectively, suggesting that these nanoparticles have promising uses in wastewater treatment. A kinetic investigation reveals that the degradation process was governed by a pseudo-first-order kinetics model, with rate constants for methylene blue and rhodamine B of 1.443

× 10^{-2} min^{-1} and 1.494 × 10^{-2} min^{-1}, respectively. Since they can both decrease electron-hole pair recombination and increase the metal oxide's ability to absorb organic contaminants, compounds derived from *Zingiber nigrum* are useful for altering metal oxides.

REFERENCES

1. Siyal, A.W., Gerbens-Leenes, P.W. and Vaca-Jiménez, S.D. (2023) *Water Resources and Industry*, 29, 100206.
2. Majumdar, A., Upadhyay, M.K., Ojha, M., Biswas, R., Dey, S., Sarkar, S., Moulick, D., Niazi, N.K., Rinklebe, J., Huang, J.-H. and Roychowdhury, T. (2024) *Science of the Total Environment*, 951, 175531.
3. Sharma, S., Sharma, V., Mittal, A., Das, D.K., Sethi, S., Yadav, S., Vallamkonda, B. and Vashistha, V.K. (2024) *Water Environment Research*, 96, e11106.
4. Sharma, B.M., Bharat, G.K., Tayal, S., Nizzetto, L., Cupr, P. and Larssen, T. (2014) *Environmental International*, 66, 48.
5. Alharbi, O.M.L., Basheer, A.A., Khattab, R.A. and Ali, I. (2018) *Journal of Molecular Liquids*, 263, 442.
6. Dutta, S., Adhikary, S., Bhattacharya, S., Roy, D., Chatterjee, S., Chakraborty, A., Banerjee, D., Ganguly, A., Nanda, S. and Rajak, P. (2024) *Journal of Environmental Management*, 353, 120103.
7. Khan, I., Saeed, K., Zekker, I., Zhang, B., Hendi, A.H., Ahmad, A., Ahmad, S., Zada, N., Ahmad, H., Shah, L.A., Shah, T. and Khan, I. (2022) *Water*, 14, 242.
8. Dire, D.J. and Wilkinson, J.A. (1987) *Journal of Toxicology - Clinical Toxicology*, 25, 603.
9. Bhatia, D., Sharma, N.R., Singh, J. and Kanwar, R.S. (2017) *Critical Reviews in Environmental Science and Technology*, 47, 1836.
10. Kusumlata, Ambade, B., Kumar, A. and Gautam, S. (2024) *Limnology and Oceanography Review*, 24(2), 126-149.
11. Samsami, S., Mohamadizaniani, M., Sarrafzadeh, M.-H., Rene, E.R. and Firoozbahr, M. (2020) *Process Safety and Environmental Protection*, 143, 138.
12. Abdelbasir, S.M. and Shalan, A.E. (2019) *Korean Journal of Chemical Engineering*, 36, 1209–1225.
13. Tripathy, J., Mishra, A., Pandey, M., Thakur, R.R., Chand, S., Rout, P.R. and Shahid, M.K. (2024) 'Water', *Water*, 16(11), 1481.
14. Asghar, N., Hussain, A., Nguyen, D.A., Ali, S., Hussain, I., Junejo, A. and Ali, A. (2024) *Journal of Nanobiotechnology*, 22, 26.
15. Ben Mbarek, W., Escoda, L., Saurina, J., Pineda, E., Alminderej, F.M., Khitouni, M., Suñol, J.-J. (2022) *Materials*, 15, 8576.
16. Ullah, E., Ye, S., Sarkar, S., Zhu, L., Meng, Z.-D. and Oh, W.-C. (2014) *Asian Journal of Chemistry*, 26(1), 145-150.
17. Gangadhar, A., Ramesh, A.M., Krishnegowda, J., Shivanna, S. (2021) *Water Practice and Technology*, 16(4), 1265–1276.
18. Din, M.I., Khalid, R., Najeeb, J. and Hussain, Z. (2021) *Journal of Cleaner Production*, 298, 126567.
19. Lee, J.-H., Lee, J.H., Kim, D.K., Park, C.-H., Yu, J.-H. and Lee, E.Y. (2016) 'J. Ind. Eng. Chem.', *Journal of Industrial and Engineering Chemistry*, 34, 157.
20. Rodrigues, T.S., da Silva, A.G.M. and Camargo, P.H.C. (2019) *Journal of Materials Chemistry A*, 7, 5857-5874.
21. Wang, S., Liu, Z., Wang, W. and You, H. (2017) *RSC Advances*, 7, 37065-37075.
22. Duman, H., Akdaşçi, E., Eker, F., Bechelany, M. and Karav, S. (2024) *Nanomaterials*, 14(22), 1805.
23. Gul, M., Kashif, M., Muhammad, S., Azizi, S. and Sun, H. (2025) *Crystal Growth & Design*, 25, 7, 2227.
24. Ali, H. and Jana, N.R. (2018) *Photochemical & Photobiological Sciences*, 17, 628-637.
25. Hu, J.Q., Wang, Z.P., Li, J. (2007) *Sensors*, 7(12), 3299–3311.
26. Bahrulolum, H., Nooraei, S., Javanshir, N., Tarrahimofrad, H., Mirbagheri, V.S., Easton, A.J. and Ahmadian, G. (2021) *Journal of Nanobiotechnology*, 19, 86.
27. Alsaiari, N.S., Alzahrani, F.M., Amari, A., Osman, H., Harharah, H.N., Elboughdiri, N. and Tahoon, M.A. (2023) *Molecules*, 28(1), 463.
28. Carmona, M., Poblete-Castro, I., Rai, M., Turner, R.J. (2023) *Microbial Biotechnology*, 16, 861.
29. Saleem, A.M., Prabhavathi, G., Karunanithy, M., Ayeshamariam, A. and Jayachandran, M. (2018) *Journal of Bionanoscience*, 12, 1–7.
30. Francis, S., Joseph, S., Koshy, E.P. and Mathew, B. (2017) *Environmental Science and Pollution Research*, 24, 17347.
31. Abdel-Raouf, N., Al-Enazi, N.M. and Ibraheem, I.B.M. (2017) *Arabian Journal of Chemistry*, 10, S3029.
32. Mata, R., Bhaskaran, A. and Sadras, S.R. (2016) *Particuology*, 24, 78.
33. Baruah, D., Goswami, M., Singh Yadav, R.N., Yadav, A. and Moni Das, A. (2018) *Journal of Photochemistry and Photobiology B*, 186, 51.
34. Hosny, M., Fawzy, M., El-Badry, Y.A., Hussein, E.E. and Eltaweil, A.S. (2022) *Journal of the Saudi Chemical Society*, 26, 101419.
35. Shahrajabian, M.H., Sun, W. and Cheng, Q. (2019) *Acta Agriculturae Scandinavica, Section B - Soil & Plant Science*, 69, 546.
36. Mao, Q.Q., Xu, X.Y., Cao, S.Y., Gan, R.Y., Corke, H., Beta, T. and Li, H.B. (2019) *Foods*, 8, 185.
37. Amalia, R.T., Tukiran, Sabila, F.I., Suyatno (2021) *Chemical Natural Acta*, 9, 14.
38. Ayustaningwarno, F., Anjani, G., Ayu, A.M. and Fogliano, V. (2024) *Frontiers in Nutrition*, 11, 1364836.
39. Patil, T.P., Vibhute, A.A., Patil, S.L., Dongale, T.D. and Arpita, P.T. (2023) *Applied Surface Science Advances*, 13, 100372.
40. Sahoo, M.K. and Sayoo, L. (2014) *Desalination and Water Treatment*, 52, 3411.
41. Tapia-Tlatelpa, T., Trull, J. and Romeral, L. (2019) *Catalysts*, 9(8), 669.

42. Shabestarian, H., Homayouni-Tabrizi, M., Soltani, M., Namvard, F., Azizi, S., Mohamad, R. and Shabestarian, H. (2017) *Materials Research*, 20, 264.
43. Donga, S., Bhadu, G.R. and Chanda, S. (2020) *Artificial Cells, Nanomedicine, and Biotechnology*, 48, 1315.
44. Piella, J., Bastús, N.G. and Puntes, V. (2016) *Chemistry of Materials*, 28, 1066.
45. Al-Maydama, H.M.A., Jamil, Y.M.S., Awad, M.A.H. and Abduljabbar, A.A.M. (2023) *Heliyon*, 10, e23722.
46. Gurunathan, S., Han, J., Park, J.H. and Kim, J.-H. (2014) *Nanoscale Research Letters*, 9, 248.
47. Ahmad, T., Bustam, M.A., Irfan, M., Moniruzzaman, M., Asghar, H.M.A. and Bhattacharjee, S. (2019) *Biotechnology and Applied Biochemistry*, 66, 698.
48. Ahmad, T., Bustam, M.A., Irfan, M., Moniruzzaman, M., Asghar, H.M.A. and Bhattacharjee, S. (2018) *Journal of Molecular Structure*, 1159, 167.
49. El-Borady, O.M., Ayat, M.S., Shabrawy, M.A. and Millet, P. (2020) *Advanced Powder Technology*, 31, 4390.
50. Akilandaeaswari, B. and Muthu, K. (2020) *Materials Letters*, 277, 128344.
51. Balasubramani, G., Ramkumar, R., Krishnaveni, N., Pazhanimuthu, A., Natarajan, T., Sowmiya, R. and Perumal, P. (2015) *Journal of Trace Elements in Medicine and Biology*, 30, 83.
52. Sunderam, V., Thiyagarajan, D., Lawrence, A.V., Mohammed, S.S.S. and Selvaraj, A. (2019) *Saudi Journal of Biological Sciences*, 26, 455.
53. Razzaq, H., Saira, F., Yaqub, A., Qureshi, R., Mumtaz, M. and Saleemi, S. (2016) *Journal of Photochemistry and Photobiology B*, 161, 266.
54. Balkrishna, A., Kumar, A., Arya, V., Rohela, A., Verma, R., Nepovimova, E., Krejcar, O., Kuca, K. (2021) *Oxidative Medicine and Cellular Longevity*, 2021, 3155962.
55. Rokkarukala, S., Cherian, T., Ragavendran, C., Mohanraju, R., Kamaraj, C., Almoshari, Y., Albariqi, A., Sultan, M.H., Alsalhi, A., Mohan, S. (2023) *Heliyon*, 9(3), e14668.
56. Amhan, S.A., Khalaf, Y.H., Mohammed, A.M. (2025) *Results in Chemistry*, 17, 102648.
57. Zayed, M.F., Mahfoze, R.A., El-kousy, S.M. and Al-Ashkar, E.A. (2020) *Colloids and Surfaces A: Physicochemical and Engineering Aspects*, 585, 124167.
58. Ali, F., Ali, S., Shahbaz, S., Summer, M., Ali, N.M.A., Farooq, M.A., Tanveer, T., Hassan, A., Shakir, H.A. (2023) *ChemistrySelect*, 8, e202301889.
59. Balaji, S. and Kumar, M.B. (2017) *Advanced Powder Technology*, 28, 785.
60. Dhanalakshmi, M. and Losetty, V. (2024) *Clean Technologies and Environmental Policy*; doi: 10.1007/s10098-024-02776-4.
61. Adewale, O.B., Egbeyemi, K.A., Onwuelu, J.O., Potts-Johnson, S.S., Anadozie, S.O., Fadaka, A.O., Osukoya, O.A., Aluko, B.T., Johnson, J., Obafemi, T.O., Onasanya, A. (2020) *Heliyon*, 6, e05501.
62. Hulikere, M.M., Joshi, C.G., Danagoudar, A., Poyya, J., Kudva, A.K., Dhananjaya, B.L. (2017) *Process Biochemistry*, 63, 137-144.
63. Bakur, A., Niu, Y., Kuang, H. and Chen, Q. (2019) *AMB Express*, 9, 62.
64. Hosny, M., Fawzy, M., El-Badry, Y.A., Hussein, E.E. and Eltaweil, A.S. (2022) *Journal of the Saudi Chemical Society*, 26, 101419.
65. Khan, I., Saeed, K., Zekker, I., Zhang, B., Hendi, A.H., Ahmad, A., Ahmad, S., Zada, N., Shah, T., Khan, I. (2022) *Water*, 14(2), 242.
66. Sharma, J., Sharma, S., Bhatt, U., Soni, V. (2022) *Journal of Hazardous* Materials Letters, 3, 100069.